

BioSNet: A Fast-Learning and High-Robustness Unsupervised Biomimetic Spiking Neural Network

Mingyuan Meng[‡], Xingyu Yang[‡], Shanlin Xiao^{*}, *Member, IEEE*, and Zhiyi Yu^{*}, *Senior Member, IEEE*

Abstract— Spiking Neural Network (SNN), as a brain-inspired machine learning algorithm, is closer to the computing mechanism of human brain and more suitable to reveal the essence of intelligence compared with Artificial Neural Networks (ANN), attracting more and more attention in recent years. In addition, the information processed by SNN is in the form of discrete spikes, which makes SNN have low power consumption characteristics. In this paper, we propose an efficient and strong unsupervised SNN named BioSNet with high biological plausibility to handle image classification tasks. In BioSNet, we propose a new biomimetic spiking neuron model named MRON inspired by ‘recognition memory’ in the human brain, design an efficient and robust network architecture corresponding to biological characteristics of the human brain as well, and extend the traditional voting mechanism to the Vote-for-All (VFA) decoding layer so as to reduce information loss during decoding. Simulation results show that BioSNet not only achieves state-of-the-art unsupervised classification accuracy on MNIST/EMNIST data sets, but also exhibits superior learning efficiency and high robustness. Specifically, the BioSNet trained with only dozens of samples per class can achieve a favorable classification accuracy over 80% and randomly deleting even 95% of synapses or neurons in the BioSNet only leads to slight performance degradation.

Index Terms—Spiking Neural Network, Unsupervised Learning, Learning Efficiency, Robustness, Image Classification.

I. INTRODUCTION

SPIKING Neural Network (SNN), as the third generation of neural network after Artificial Neural Network (ANN), is attracting growing interest of researchers due to its biomimetic nature, low-latency computing mechanism, and high energy-efficiency[1]. At present, there are two approaches for the research of advanced SNN [2]: one is biomimetic modeling research based on neuroscience and the other is machine learning research oriented by computer science. However, most of the current SNN research tend to be oriented by computer science

and lack the underlying foundation of biological structure and rules. In order to obtain a superior SNN, we combine these two approaches. Specifically, we design effective biomimetic spiking neuron model and network architecture based on neuroscience while refine the learning methods and encoding/decoding mechanism oriented by computer science.

The SNN algorithms for image classification can be divided into three categories: supervised [3], unsupervised [4], and semi-supervised [5], as investigated in TABLE I. The supervised algorithms utilize the output of the SNN as instructor signal and adjust the synaptic weight to minimize the error function of the actual output and the target output. The unsupervised algorithms let the neurons adjust their own synaptic weights according to their own activities, which is similar to the process of real neurons in human brain [6]-[7]. The semi-supervised algorithms are combinations of two categories, consisting of partial supervised algorithms and partial unsupervised algorithms. Admittedly, the most research of SNN is developing supervised SNN algorithms and the present supervised SNN algorithms have yielded superior classification accuracy than unsupervised/semi-supervised SNNs. However, since there is no instructor signal in the human brain and the learning of the human brain can be regarded as unsupervised learning [8], the unsupervised SNN is considered to possess more biological plausibility and more potential to imitate human brain.

In addition to the above algorithms of directly training SNN, some researchers proposed the methods of converting trained ANN to SNN [9], in which an ANN is trained first, and then its connection weights are utilized in the SNN with same network architecture. Since the original ANN needs to be pruned before training and there is information loss in the conversion of the ANN into the SNN [10], such methods make the converted SNN lose the potential to surpass ANN.

Spiking neuron model also is an important element of SNN algorithms. The earliest SNN model is Integrated-and-Fire (IF) RC circuit neuron model. Because of the ion diffusion effect of real neurons, the leaky current term is introduced to the basic model and a Leaky Integrate-and-Fire (LIF) model was proposed (‘Leaky’ means that the membrane potential of neuron decays as time goes on). Moreover, as investigated in TABLE

Manuscript received October 30, 2019. This work was supported in part by grants from National Key R&D Program of China 2017YFA0206200, 2018YFB2202601 and National Nature Science Foundation of China (NSFC) under grant No. 61674173, 61834005 and 61902443. (‡ M. Meng and X. Yang contribute equally to this paper. * S. Xiao and Z. Yu both are corresponding authors.)

M. Meng, X. Yang, S. Xiao, and Z. Yu are with the School of Electronics and Information Technology, Sun Yat-sen University, Guangzhou, 510006 China (e-mail: mengmy3@mail.sysu.edu.cn, yangxy266@mail2.sysu.edu.cn, xiaoshlin@mail.sysu.edu.cn, yuzhiyi@mail.sysu.edu.cn).

TABLE I
INVESTIGATION ON PREVIOUS SNN ALGORITHMS

Paper	Category	Description
Xie et al. 2016 [11]	Supervised	Accurate synaptic-efficiency adjustment method
McKeanoch et al. 2006 [12]	Supervised	Spikeprop
Ponulak et al. 2010 [13]	Supervised	ReSuMe
Wade et al. 2010 [14]	Supervised	SWAT
Diehl et al. 2015 [15]	Unsupervised	Fully-connected SNN with STDP
Daniel et al. 2019 [16]	Unsupervised	Locally-connected SNN with STDP
Panda et al. 2018 [17]	Unsupervised	Adaptive synaptic plasticity (ASP) and STDP
Falez et al. 2019 [18]	Semi-supervised	Target timestamp threshold adaptation and STDP + SVM
Tavanaei et al. 2017 [19]	Semi-supervised	Multi-layer SNN with STDP + SVM
Kheradpisheh et al. 2018 [20]	Semi-supervised	Multi-layer SNN with STDP + SVM

TABLE II
INVESTIGATION ON SPIKING NEURAL MODELS

Name	Category	Description
Hodgkin et al. 1952[21]	Membrane potential model	Highly biomimetic with complex differential calculation
Izhikevich et al. 2003[22]	Membrane potential model	Potential negative feedback with changeable parameters
Jeyasothy et al. 2018[23]	Membrane potential model	Supervised STDP learning with SRM
Nossenson et al. 2016[24]	Natural information input model	Gaussian-signal-in-Gaussian noise (model-based) detector
Fan et al. 2015 [25]	Hierarchical temporal memory model	Identifies patterns require computationally expensive tasks

II, the Hodgkin-Huxley (HH) model [21] is proposed through measuring the squid axon potential by voltage clamp and derived a series of improved neuron models such as Izhikevich model [22]. The Spike Response Model (SRM) is an extension of IF model [23], so the LIF model can also be mapped into an SRM. The current spike neuron models used in SNN are mainly IF model, LIF model, and their corresponding SRM models. The models mentioned above all are membrane potential models, however, in the human brain, there are two kinds of synapses: electrical synapses and chemical synapses, meaning that, besides the electrical model, the neuron model can be extended to other types of models like natural information input model [24], hierarchical temporal memory model [25], and so on.

The currently existing neuron models act inflexibly due to the independence of their responding process to information and separately processed parameters in them, limiting the information utilization. Their bound innate structures hinder the performance improvement of the network, which motivates us to construct a new flexible neuron model with more biological plausibility. Besides, in order to improve the learning and recognition capabilities, previous SNN algorithms with increasing network depth and complicated architecture lead to a larger number of learning samples and a longer training time needed

[17]-[20], which also encourages us to design a biomimetic network architecture with prominent biological characteristics of the human brain.

In this paper, inspired by the learning and computing characteristics of the human brain, we proposed a highly biomimetic unsupervised SNN named BioSNet. It not only performs prominent learning efficiency and high robustness but also possesses strong biological plausibility. Our network achieves state-of-the-art result among current unsupervised SNN algorithms for image classification tasks on the MNIST/EMNIST data sets. The proposed BioSNet mainly has three contributions respectively in spike neuron model, network architecture, and decoding mechanism, respectively: 1) A new flexible spiking neuron model named MRON (Memory Reserved neurON). Inspired by the 'recognition memory' [26] of the human brain, we introduce the membrane potential retention behavior of brain neuron to MRON and the memory of the previous information's type for a period of time is preserved to be used in the future process of information. It's shown that MRON improves the classification accuracy and learning efficiency. 2) An efficient and robust network architecture based on the parallelism and redundancy characteristics of the human brain. Combined with our proposed Area-Competitive Learning (ACL), this network architecture improves the learning efficiency and robustness, enabling the BioSNet trained with only dozens of samples per class or suffering from random neuron/synapse deletion with 95% probability to still exhibit favorable classification performances. 3) An effective decoding mechanism designed to reduce the information loss in the process of output decoding. We call it Vote-for-All (VFA) voting mechanism and implemented it as a network layer named VFA decoding layer, which also enhances the classification performance of our BioSNet.

II. MOTIVATIONS

A. Bio-inspired Neuron Model

The human has a certain memory of the environment and things around him/her in the consciousness, and the memory gradually fades as time goes on. When the human is faced with the same or similar things again, the deep subconscious memory will be stimulated, thus enhancing the brain's ability to recognize and respond. Therefore, the human will feel familiar to these things due to the previously kept memory in the brain and this kind of memory is called 'recognition memory'. Similarly, we hope the spike neurons preserve the memory of the information's type after processing it, so that this neuron can recognize and process more quickly when receiving the same type of information again.

Therefore, inspired by the 'recognition memory' of the human brain, we design a simple but efficient spiking neuron model named MRON (Memory Reserved neurON) possessing the similar memory effect. Concretely, a membrane potential preserved self-adaptive neuron model based on the incremental changes of the transmitter was designed, which makes the information of the past period of time act in the present and later responding process in the form of transiently transformed membrane potential. Moreover, because the discharge (namely fire a spike) capacity of each neuron is different, and the neurons in the refractory period can still accept the signal (spike) and per-

form local depolarization, we design the MRON to perform hyperpolarization or depolarization according to the preserved memory of previous information's type when discharging. Besides, synaptic release of real neurons is quantized, the total amount of synaptic release is variable for a certain neuron and exhibits much more discrepancy among different neurons [27]. So, in BioSNet we quantify the synaptic release of MRON in the form of exponential fluctuations. Please read Section III-A for the details of MRON model.

B. Efficient and Robust Network Architecture

The human brain is considered to be an amazing learning and computational system that is worth researching and imitating, not only because it has a very superior ability to handle abstract and complex tasks, but also because it has extremely fast learning speed and ultra-high robustness against external interference and damage. Specifically, when facing cognition and classification tasks, the human brain can not only utilize very limited learning samples to quickly grasp the internal similarities and features of them but also show amazing performance even with external interference and damage. The internal architecture of the human brain is characterized by parallelism and redundancy [28], meaning there are many similar structures learning in parallel and performing similar functions in the human brain, which actually is the reason for its extremely fast learning speed and ultra-high robustness. In contrast, current deep learning methods tend to increase the depth of a single feedforward network and complicate the structure of it in order to improve its learning and recognition capabilities [29], leading to a large number of learning samples and a long training time needed to get a well-trained network. This trend also makes the network's learning ability highly dependent on its deep, complex multi-layer architecture, which reduces network robustness because complex computing systems without any backup surely are vulnerable to external interference and damage.

In this paper, inspired by the internal architecture of the human brain, we design a biomimetic SNN architecture with surprising learning efficiency and high robustness, in which we increased the width of the network but reduced the depth. Specifically, our network consists of three parallel channels and each channel is much shallower (meaning fewer layers and filters included in this channel) than other popular SNN architecture [15]-[20]. These three channels perform similar functions but have different topology parameters to process features in different scales. In addition, we also propose ACL, dividing the whole network into several sub-networks that can learn and run in parallel to further improve the learning efficiency and robustness of the network. Please read Section III-B and Section III-C for the details of our network architecture and ACL.

C. Effective Decoding Mechanism

When applying the trained SNN to image classification tasks, we need to decode the output spike trains to attain the predicted results. At this time, an effective decoding mechanism can better extract the result information from the output spike trains, thereby significantly improving the classification performance. In general, unsupervised SNNs with rate-based input encoding

use the voting mechanism for output decoding [15]-[16], because the information processed by this type of SNN has been encoded into the rate of the spike trains and the voting mechanism can count the number of spikes emitted by each output neuron (Apparently, the number of spikes is proportional to the rate of the output spike train) to build the relationship between the output spike trains and the classification results. Specifically, the traditional voting mechanism is: First, assign a class to each output neuron based on its highest response to all classes of image over all training samples. Then, during classification each spike emitted by an output neuron is a single vote for the class assigned to this neuron. Finally, the class having the most votes is the predicted result of classification.

Obviously, the voting mechanism mentioned above causes information loss, because only one class is assigned to each output neuron but each output neuron is not only responsive to a single class in reality. For example, an output neuron may have strong responses for images in several classes. If we only assign one class to this output neuron based on its highest response, all spikes of this neuron will be considered as votes for this single class, resulting in information loss in decoding process. In order to avoid information loss in this process, we propose VFA voting mechanism and realized it as a network layer named VFA decoding layer. In this paper, we use VFA decoding layer as output layer in our designed BioSNet. The main distinction of VFA voting mechanism is that each output neuron votes for all classes (That's why we call it Vote-for-All), but the number of votes for each class depends on neuron's response to each class. Please read Section III-D for the details of VFA decoding layer.

III. BIOSNET DESIGN DETAILS

A. MRON Model and STDP Rule

1) MRON Modeling

In this section, the proposed MRON (Memory Reserved neuron) model is described in detail. The currently existing neuron models, such as the HH model, the LIF model, and the Izhikevich model, specify the actions of neurons in the constraints of their modeling processing, and lack the strain capacity and correction ability in some way. The existing neuron models don't retain and utilize their state variables of the previous moment after they fire a spike and when they prepare to enter the same phase of change in the next process. However, MRON applies the amount of transmitter changed over a period of time to adjust its membrane potential. We refer to neurotransmitter, neuropeptides, and other types (such as NO, CO, etc.) as transmitter, and use the formulas that conform to the general variation rules to quantify transmitter. The MRON model is defined as follows:

$$v_t \text{ is: } \begin{cases} v_0 & 0 \leq t < t_1 \quad (f=0) \\ \sum_{i=1}^{N_{pref}} v_{pref}^{\wedge} \cdot \exp\left(-\frac{t-t_i}{\tau_v}\right) & t_i \leq t < t_f \\ \eta(t - t_f^{\wedge}) + C_{rest} + \Delta v_{MRON} & t_f^{\wedge} \leq t \end{cases} \quad (1)$$

where C_{rest} is a voltage constant indicating the resting potential, τ_v is the time constant of neuron potential, and N_{pref} represents the number of all the pre-synapses which connected to the

postsynaptic neuron, v_0 is the initial value of membrane potential, t_i represents the time node of the first spike of one synapse (namely i_{th}) in N_{pref} , and t_f is the time when the neuron fires a spike. When the neuron's membrane potential reaches or exceeds potential threshold $C_{v_{thr}}$, it emits a spike to downstream neuron and enter a refractory period $\eta(t - t_f)$. At the end of refractory period, the potential v_t will return to C_{rest} and then make a certain adjustment Δv_{MRON} of potential.

And, the v_{pref} triggered by the i^{th} spike:

$$v_{pref} = \Delta v_{t_{fire}} \int_{t_{i+*}}^t \delta_{i+*} \cdot dt \quad t \geq t_i \quad (2)$$

There are two types of synapses in human brain: excitatory synapse and inhibitory synapse. Excitatory pre-synapses triggers EPSP (excitatory postsynaptic potential) and inhibitory pre-synapses triggers IPSP (inhibitory postsynaptic potential). In conductance-based SRM neuron model, the transmitter actually is excitatory/inhibitory conductance respectively emitted by excitatory/inhibitory pre-synapses.

The transmitter's type is not limited to conductance but can be other forms, and the quantification forms of transmitter can be different too. To describe the transmitter in the transmitting path (synapse), here we define the time-dependent δ_i as follows:

$$\delta_{i(t)} = C_i \omega_i \exp\left(-\frac{t-t_i}{\tau_i}\right) \quad t - t_i \geq 0 \quad (3)$$

where $\delta_{i(t)}$ represents transmitter transmitted by one synapse. Similar to the sudden rise of the neurotransmitter when the real neuron's electrical signal arrives, when the spike is emitted, δ_i start from the maximum and then decays exponentially in general. It needs be noted that when one synapse emits more than one spike, synapses on the timeline will be treated as multiples like t^* in Fig. 1 while $t_3 < t^* < t_4$ (consistent with the spikes number). In order to keep the synapses and the spikes in a one-to-one relationship, when a synapse emits more than one spike, the extra spikes will be treated as virtual synapses like t^* in (2). In conductance-based neuron, τ_i is the time constant of conductance change, C_i is a constant indicating the transmitter reception degree of the neuron at the end of the path, transmitter of different pre-synapses may be accepted in different degree. To simplify the experiment, it is defaulted to 1, namely all received. And we use the connection weight value ω_i to describe the neuron's inside receiving probability of presynaptic spikes. It can be adjusted according to the actual situation.

The $\Delta v_{t_{fire}}$ in (2) is the potential difference of post-synaptic neuron when it receiving spike signals:

$$\Delta v_{t_{fire}} = E_{eq} - v_{t_{fire}} \quad (4)$$

where E_{eq} is the reverse ionic equilibrium potential of the synapse but exists only in inhibitory synapses, $v_{t_{fire}}$ is the membrane potential at spike receiving time. In BioSNet, we set the E_{eq} between -100mV and -80mV like real neurons. The overall effect Δv_{pref} is the result of the interaction of EPSP and IPSP. For all transmitter increments passed to a certain neuron, the dominant transmitter with a certain type retains its same type of

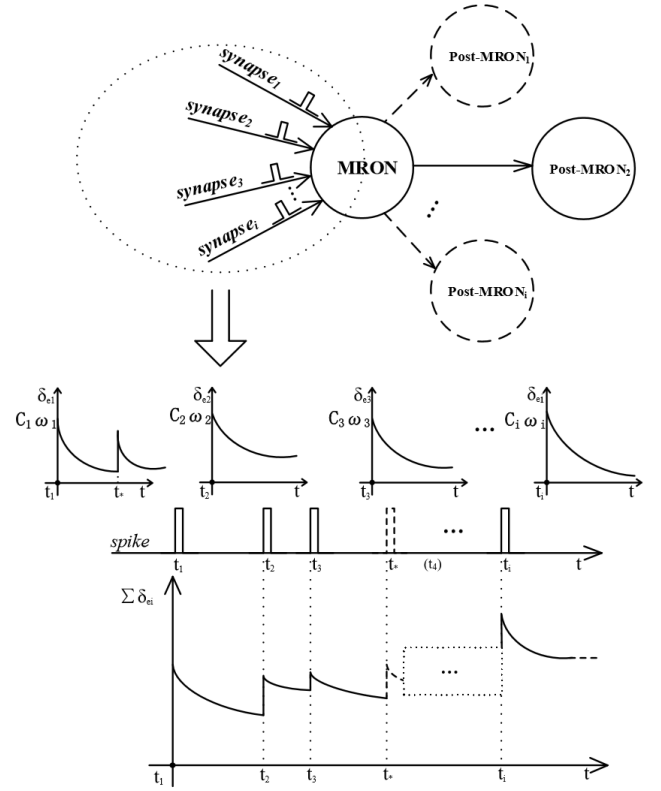


Fig. 1. The number of synapses connected to a single MRON is N_{pref} , and this MRON counts the total amount of excitatory and inhibitory transmitter in synaptic transmission of all pre-synapses.

effect on the membrane potential. That is, the membrane potential memory adjustment that retains the same properties according to the properties of the dominant transmitter, equivalent to joining depolarization and hyperpolarization effects.

The Δv_{MRON} is the memory potential adjustment of MRON model. As shown in Fig. 1, for postsynaptic neuron, the total amount of transmitter of the same category received in N_{pref} is:

$$\delta_{\Sigma i} = \sum_{i=1}^{N_{pref}} C_i \omega_i \exp\left(-\frac{t-t_i}{\tau_i}\right) \quad t - t_i \geq 0 \quad (5)$$

$\delta_{\Sigma i}$ is derived from the superposition of each synaptic transmitter. Then, we set the time node of the last (relative to this time) spike fired to t_0 , and the event status is recorded as A_0 . This time of the spike fired is set to t , and the event status is recorded as A .

For A_0 , the total amount of different types of transmitter are:

$$\delta_{\Sigma exc}^0 = \sum_{d=1}^m C_d \omega_d \exp\left(-\frac{t-t_d}{\tau_1}\right) \quad t_d \leq t < t_0 \quad (6)$$

$$\delta_{\Sigma inh}^0 = \sum_{j=1}^n C_j \omega_j \exp\left(-\frac{t-t_j}{\tau_2}\right) \quad t_j \leq t < t_0 \quad (7)$$

For A , they are:

$$\delta_{\Sigma exc} = \sum_{d=1}^m C_d \omega_d \exp\left(-\frac{t-t_d}{\tau_1}\right) \quad t_0 < t_d \leq t \quad (8)$$

$$\delta_{\Sigma inh} = \sum_{j=1}^n C_j \omega_j \exp\left(-\frac{t-t_j}{\tau_2}\right) \quad t_0 < t_j \leq t \quad (9)$$

where m and n are the number of excitatory pre-synapses and

inhibitory pre-synapses in N_{pref} respectively, τ_1 and τ_2 are the decay time constant of excitatory and inhibitory conductance. In all the signals (spikes) received by a certain neuron, the time series of spikes triggered by excitatory presynaptic neurons and transmitted by the excitatory pre-synapses is $\{t_d, d \in m\}$, the time series of spikes triggered by inhibitory presynaptic neurons and transmitted by the inhibitory pre-synapses is $\{t_j, j \in n\}$.

$$\Delta\delta_{e,i} = (\delta_{\Sigma exc}^0 - \delta_{\Sigma exc}^0) - (\delta_{\Sigma inh}^0 - \delta_{\Sigma inh}^0) \quad (10)$$

$$\Delta v_{MRON} = \alpha \cdot \Delta C \cdot (\Delta\delta_{e,i} > 0) - \alpha \cdot \Delta C \cdot (\Delta\delta_{e,i} < 0) \quad (11)$$

$$\Delta C = C_{v_{thr}} - C_{rest} \quad (12)$$

where the α is the memory effect coefficient, ranging from 0% to 100%. In BioSNet, we set C_{rest} to -65mV, the general resting potential of most neurons, and set $C_{v_{thr}}$ to -52mV, a membrane potential threshold near for nerve fibers.

Fig. 2 shows a schematic diagram of the approximate membrane potential, and the actual spike emission density is larger. When the property (type) of the dominant transmitter received by the neuron is excitatory, the neuron firing spike retains a certain degree of positive potential, simulating local depolarization. When this is inhibitory, the neurons retain a negative potential when they emit spikes, simulating local hyperpolarization.

Through membrane potential adjustment, the competitiveness of some neurons after discharge is enhanced and realized self-discipline, and the EPSP and IPSP are verified again to be related to the release amount of the transmitter. We set α to a percentage in steps of 10%, and take the integer approximations of $\alpha \cdot \Delta C$. The experimental results show that the MRON model improves the amount of partial spike triggering with a stable trend, reduces latency, accelerates the learning efficiency and enhances the overall recognition accuracy of BioSNet for the MNIST/EMNIST. Then, in the experiment, we found that the improvement of network performance gradually fades with the increase of the network scale and the number of the training

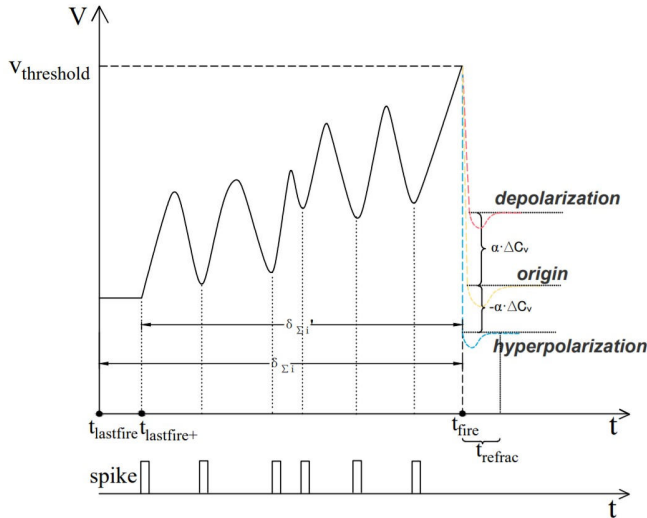


Fig. 2. The Variation of membrane potential in a single MRON from the time of last spike $t_{lastfire}$ to the time of current spike t_{fire} . The MRON launches the polarization after t_{fire} according to the amount of transmitter it has received.

samples when the memory effect coefficient α is a fixed value, which increases the difficulty of further improving the network performance.

Through experiments, it is found that there is a phenomenon that the competition intensity becomes more weakness in the process with increasing samples. Therefore, we further improve the method and set α to the inverse exponential decay form, in which α decreases as the network's training goes on. We set α as follows:

$$\alpha = X^{i-n} \quad (13)$$

where X is the base number of α , i is a variable which increases from 0 to n as the network's training goes on. However, in order to avoid the extreme boundary conditions, in BioSNet, we perform the piecewise linearization for the change of α according to a certain sample interval:

$$\alpha = \{X^{1-n}, X^{2-n} \dots X^{n-n}\} \quad (14)$$

where $fund$ is the length of the interval, and n is the multiple of the total number of training samples to the $fund$. We set $X=0.5$, $fund=2 \times 10^4$ in BioSNet and make α decrease each time the network is trained with $fund$ training samples.

2) STDP Rule

We use a basic STDP to adjust synaptic weights between neurons. In order to improve the overall simulation speed of our network, the STDP rule is simplified as follows:

$$\Delta\omega = \begin{cases} A_1 \cdot x_{pre} \cdot x_{post2} & \text{when postsynaptic spike} \\ -A_2 \cdot x_{post1} & \text{when presynaptic spike} \end{cases} \quad (15)$$

where A_1 and A_2 are learning rates respectively for postsynaptic and presynaptic spike events, ω represents synaptic weight, and x indicates synaptic traces used to compute weight dynamics [30]. Presynaptic trace (x_{pre}) and postsynaptic traces (x_{post1} , x_{post2}) are set to 1 respectively on presynaptic and postsynaptic spike events, otherwise they decay exponentially with τ_{pre} , τ_{post1} , and τ_{post2} as their time constant respectively. The use of these synaptic traces is actually equivalent to recording the timing of the latest presynaptic or postsynaptic spike. To emphasize the effect that presynaptic neuron has on postsynaptic neuron, we set $A_1 \gg A_2$. In the BioSNet, we set $A_1 = 0.01$, $A_2 = 0.0001$, $\tau_{pre} = 20ms$, $\tau_{post1} = 20ms$, and $\tau_{post2} = 40ms$ as a default.

B. Network Architecture

Fig. 3 shows a comprehensive network architecture of our proposed BioSNet. As is shown in Fig. 3, there are three kinds of layers in BioSNet: input layer, Locally-Connected layer (LC layer), and VFA decoding layer. The input layer and LC layer are utilized in three channels that learn and run in parallel to improve the learning efficiency and robustness of BioSNet, while the VFA decoding layer, also as the output layer, integrates information from three channels and decodes spike trains from the LC layers into readable predicted classification results.

The input layer is used to encode the analog pixel values of image into the discrete spike trains and each node of this layer

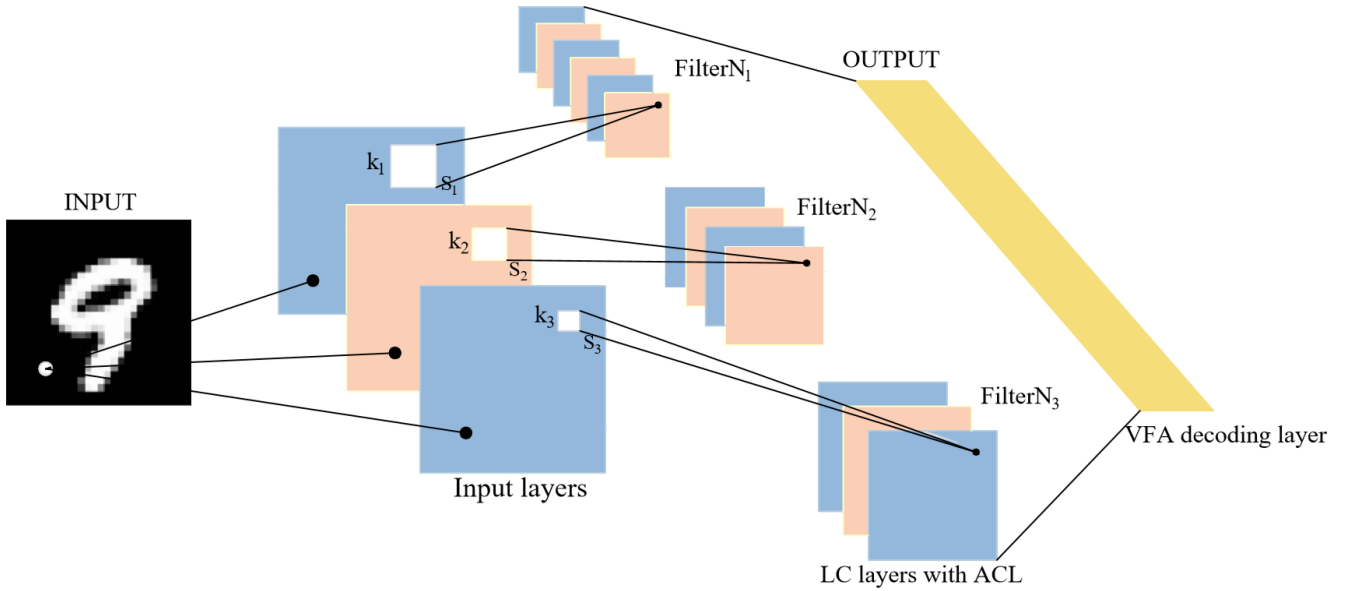


Fig. 3. A comprehensive network architecture of our proposed BioSNet consisting of three parallel data processing channels with different topology parameters. Each channel is composed of an input layer and a LC layer complying with ACL rules, while a VFA decoding layer (output layer) is utilized to integrate multi-channel information.

corresponds to a pixel of the input image. Because BioSNet utilizes rate-based input encoding mechanism, each node of the input layer is a generator of Poisson-distributed spike trains. For the input layer in the i^{th} channel, when its nodes receive non-negative pixel values of input image, they output Poisson-distributed spike trains whose average rates are equal to corresponding pixel values multiplied by an encoding parameter λ_i . Note that there are three input layers respectively in three channels instead of a single input layer connected to three LC layers, because λ_1 , λ_2 , and λ_3 should be allowed to be different or even respectively adaptive in each channel (Read Section III-E for the strategy of adaptive encoding parameter).

The LC layer is composed of MRON models and connected to the input layer with STDP-modifiable synapses (meaning the synapse that adjusts its own synaptic weight according to STDP rule). The concept of LC layer is borrowed from the deep learning literature [31] and implemented in SNN firstly by [16]. A closely related concept is the convolutional layer whose weights are shared between locations in the input space. The LC layer has the same connections architecture as the convolutional layer, but it doesn't have shared weights. Similarly, the LC layer uses topology parameters including kernel size (denoted by k), stride length (denoted by s), and the number of filters (denoted by $FilterN$) to determine its connections topology and the number of neurons included in a filter (denoted by $FilterS$). In our BioSNet, three LC layers should have different topology parameters to extract features of different scales so as to improve the overall classification performance. Therefore, in the following part of this paper, we use (k_1, k_2, k_3) , (s_1, s_2, s_3) , $(FilterN_1, FilterN_2, FilterN_3)$, and $(FilterS_1, FilterS_2, FilterS_3)$ to denote the properties of three channels in BioSNet. Moreover, besides the STDP-modifiable synapses between the input layers and the LC layers, there are still fixed inhibitory synapses complying with ACL rules between the neurons

within the same LC layer.

C. Area-Competitive Learning (ACL)

The learning function of the BioSNet stems from competitive learning procedures [32] like self-organizing maps [33] or neural-gas [34]. The main idea of competitive learning is that each neuron learns and represents one prototypical input (which is initialized randomly and gradually become more similar to the real inputs through learning). Every time a training sample is input, the neurons compete with each other and only the one whose represented prototypical input is most similar to this input sample can fire spikes and adjusts its synaptic weights based on STDP rules to make its represented prototypical input even more similar to this input sample. Those winner neurons are finally used to predict the class of the input sample because they respond so much to the input samples that are similar to their represented prototypical inputs.

Our proposed ACL is a refined version of the traditional competitive learning, in which the neurons are placed into several areas and each neuron only competes with other neurons in the same area. As for the LC layer utilizing ACL, because its neurons have been placed into each filter, we only need to group the adjacent filters as an area from the first filter to the last one. Specifically, we define $Size_{ACL}$ as the maximum number of the filters that could be included in an area and we have the following equation:

$$AreaN = \lceil FilterN / Size_{ACL} \rceil \quad (16)$$

where $AreaN$ is the number of areas. All areas except for the last one include $Size_{ACL}$ filters and the last area might include fewer filters if $FilterN$ isn't divisible by $Size_{ACL}$. After being placed into the areas, the neurons of the LC layer are connected to other neurons that not only share the same receptive field but

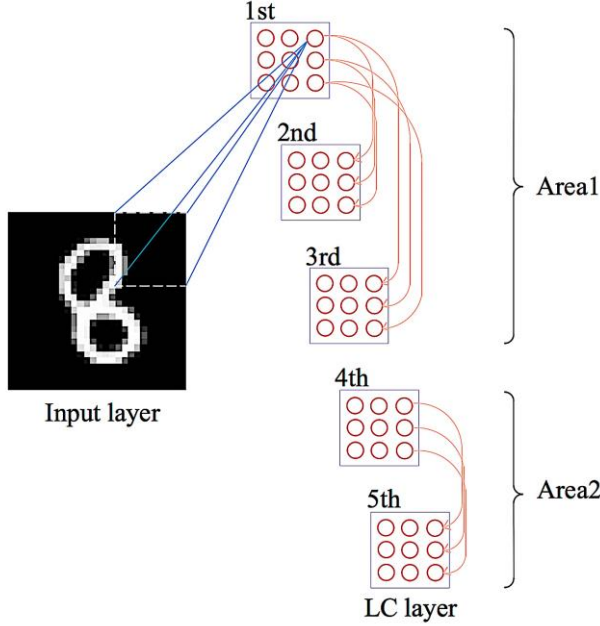


Fig. 4. Example of a simple LC layer complying with ACL rules. The related parameters ($FilterN = 5$, $FilterS = 9$, and $Size_{ACL} = 3$) are set here for an easily understandable illustration.

also are located in the same area with the fixed inhibitory synapses.

Let's take the LC layer in Fig. 4 as an example: Fig. 4 shows a very simple LC layer complying with ACL rules and the squares in Fig. 4 represent the filters of the LC layer. For providing an easily understandable illustration, we set $FilterN = 5$, $FilterS = 9$, and $Size_{ACL} = 3$ here. Therefore, these filters are divided into two areas including 3 and 2 filters respectively. As can be seen in Fig. 4, the neurons in the 1st filter are only connected to the neurons in the 2nd or 3rd filter because these three filters are in the same area. For the same reason, the neurons in the 4th filter also are only connected to the neurons in the 5th filter. Besides, the two connected neurons are located in the same position of the filter, meaning that these two connected neurons share the same receptive field.

D. VFA Decoding Layer

The VFA decoding layer is an implementation of our proposed VFA voting mechanism and is used in the BioSNet to integrate information from three channels and decodes spike trains from the LC layers. Every neuron in the VFA decoding layer represents a class, so the number of neurons in this layer is equal to the number of all possible classes in target classification task. The neuron model used in VFA decoding layer is a specially designed voltage-based non-leaky neuron model whose threshold is set to be infinite, meaning this neuron has no ability to fire spike and its potential increases from 0 to infinity when it receives spikes. Actually, this neuron serves as a vote counter to accumulate votes from the LC layers. The class represented by the neuron whose final potential is the highest is the final predicted classification result.

As is shown in Fig. 5, because 'Vote-for-all' means each neu-

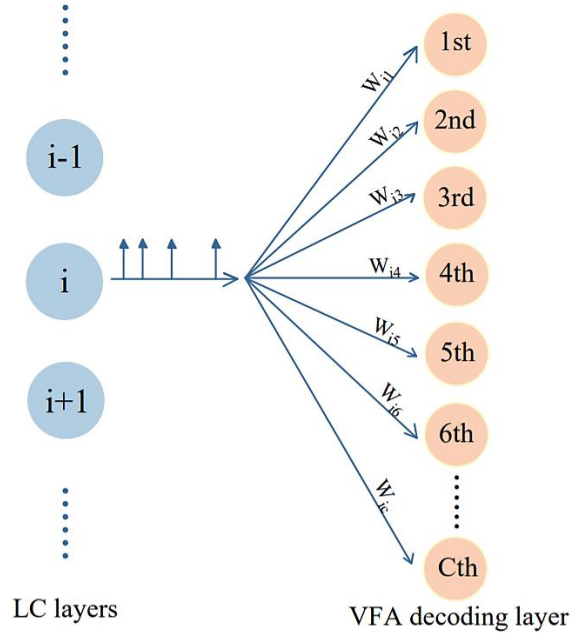


Fig. 5. Connection architecture of VFA decoding layer: the VFA decoding layer is connected to three LC layers in a fully-connected fashion to integrate votes from all pre-synaptic neurons.

ron in the LC layers needs to vote for all classes, the VFA decoding layer is connected to the LC layers in a fully-connected fashion to receive votes from all pre-synaptic neurons. The weights of the synapses are fixed to be 0 when training the network, which means the VFA decoding layer actually is excluded because it won't receive any spike at all. However, this won't cause any problem because we train our BioSNet in an unsupervised fashion and no result information is needed when training. After the training is finished, we need to update the synaptic weights of the VFA decoding layer based on the LC layers' responses to each training sample. We define the weight of the synapse between the i^{th} neuron of all three LC layers and the j^{th} neuron of VFA decoding layer as w_{ij} and w_{ij} can be calculated through:

$$w_{ij} = \frac{s_{ij}^{\mu}}{\sum_{k=1}^C s_{ik}^{\mu}} \quad (17)$$

where μ is a constant that we set to a value less than 1 through empirical research, C represents the number of all possible classes as well as the neurons in the VFA decoding layer, and s_{ij} represents the average number of spikes emitted by the i^{th} neuron in the LC layers during the training of the samples belonging to the j^{th} class.

E. Training and Classification

Fig. 6 is a flow chart for illustrating the training and classification of our BioSNet. When training the BioSNet, this network is actually learning by itself, in which we just need to input the training samples into the network one by one and let the network run for a fixed time that is defined as T_{training} (the time needed to train the network with a single sample). In this process, we don't need any label information to interfere with the

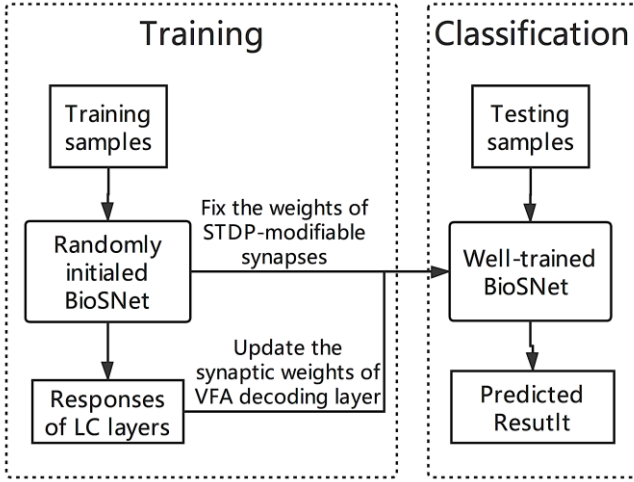


Fig. 6. A flow chart for the training and classification of BioSNet.

network training, but we need to record the LC layers' responses to each training sample to update the synaptic weights of VFA decoding layer later. After the training is finished, we fix the weights of STDP-modifiable synapses. Then, we update the synaptic weights of the VFA decoding layer based on the previously recorded responses of the LC layers. Finally, we get a trained BioSNet.

If we want to apply a well-trained BioSNet to the image classification tasks in reality, we only need to input the unclassified image into the trained BioSNet and let it run for a period of time that is defined as *Latency* (the time when we allow the network to run to attain predicted result after inputting an image). Then, the predicted classification result is presented in the VFA decoding layer. Note that, no matter whether we train the network or apply the trained network to classification, we need to reset the network after each iteration, returning all variables of the network to their initial values except for the learned weights of STDP-modifiable synapses.

In addition to the simple training scheme described above, we have also utilized some well-designed training strategies to improve the classification performance of the BioSNet:

1) Adaptive Encoding Parameter

Since the network may be insensitive to some training samples and larger encoding parameter λ are required at this time, we use adaptive encoding parameters: First, define a gate G_i for the i^{th} channel and its value is:

$$G_i = \alpha \times AreaN_i \times FilterS_i \quad (18)$$

where α is a constant that determines the resistance of G_i , and $AreaN_i$ is the number of areas in the i^{th} channel. When a training sample is encoded and input into the i^{th} channel, if the number of spikes emitted by the LC layer in this channel during $T_{training}$ is less than G_i , a constant λ_{plus} will be added to λ and this sample will be encoded for training again. The above process is repeated until the number of spikes exceeds G_i . Finally, the next training sample is input after returning λ to its initial value. In the BioSNet, as a default, we set the initial value of λ to 0.25 and λ_{plus} to 0.125 through empirical research.

2) Adaptive Potential Threshold

In order to ensure that no neuron can emit excessive spikes and dominate the firing activity of the whole layer, which would lead to the failure of area-competitive learning, we make the potential threshold $C_{v_{thr}}$ of the MRONs in the LC layers become adaptive. For realizing it, an adaptive variable θ is added to the original potential threshold $C_{v_{thr}}$. This θ is set to 0 initially and decay exponentially as time goes on. When a spike is fired, θ will increase by a constant θ_{plus} . If the i^{th} spike is fired at t_i and the θ increases to θ_i at t_i , this adaptive variable θ has dynamics as following:

$$\theta = \begin{cases} 0 & t < t_1 \\ \theta_i \exp\left(-\frac{t-t_i}{\tau_\theta}\right) & t \geq t_i \quad (i = 1, 2, 3, \dots) \end{cases} \quad (19)$$

where τ_θ is the time constant of θ . In the BioSNet, we set $\tau_\theta = 1 \times 10^7 ms$ and $\theta_{plus} = 0.05 mV$ as default through empirical research. Note that, just like the weights of STDP-modifiable synapses, the adaptive θ also shouldn't be reset after each iteration and the final θ s of all neurons need to be fixed after the training.

3) Weight Normalization

We conduct weight normalization for the STDP-modifiable synapses after each iteration of training, in which the sum of weights incident to a post-synaptic neuron is normalized to be equal to c_{norm} (a normalization constant that is different for each channel). Besides, in order to balance the activity intensity of three channels, each channel's c_{norm} needs to be dynamically adjusted to make the average number of spikes emitted by each channel equal.

4) Dropout

In order to further improve the robustness and classification performance of the BioSNet, we used channel-level's dropout: each channel skips current iteration and stays fixed with possibility ρ , which allows each channel to be trained with different data set. It's found in the experiments that the values of ρ in [2/3, 5/6] contribute to better performances.

IV. RESULTS

In order to test and verify the performances of our BioSNet, we tested the BioSNet on the MNIST data set [35] and the letters partition of the EMNIST data set [36]. The MNIST data set contains 70,000 handwritten digital images (60,000 images in training set and 10,000 images in testing set) and these images are separated into 10 classes from 0 to 9. The EMNIST data set is an extension of MNIST to handwritten letters so it's considered as a tougher task than the MNIST. There are six partitions in the EMNIST data set. Among them, the letters partition contains 145,600 handwritten letter images (124,800 images in training set and 20,800 images in testing set) and these images are separated into 26 classes corresponding to the 26 capital letters of the English alphabet.

Considering that all images in the MNIST and EMNIST are 28*28 in size, in the experiments we set the topology parameters of our BioSNet as following: $(k_1, k_2, k_3) = (28, 24, 16)$, $(s_1, s_2, s_3) = (1, 4, 6)$, and $Size_{ACL} = 400$. All these parameters are empirical values. Because the channel with larger receptive field exhibits higher classification accuracy but lower

learning efficiency, and vice versa, we distinguish three channels and combine their strengths, in which the (k_1, k_2, k_3) and (s_1, s_2, s_3) are set to make the BioSNet possess both good learning efficiency and high classification accuracy. The $Size_{ACL}$ also is set to balance the learning efficiency and classification accuracy. The $Size_{ACL}$ less than 400 leads to a slight degradation in classification accuracy, while the $Size_{ACL}$ more than 400 would make the BioSNet need to be trained with more than one single pass through the training data to achieve its best classification accuracy.

Besides, we also set $T_{training}$ as 350ms and $Latency$ as 300ms in the experiments. Actually, SNNs are known to exhibit a so-called accuracy-latency-tradeoff [37]-[38], which means that if we allow SNNs to run for a longer $Latency$, they will perform a better classification accuracy. Therefore, choosing a longer $Latency$ can make the BioSNet show better performances. However, too long $Latency$ is unacceptable in some real-time applications and the $Latency$ used in the experiments is a tolerable one for most of applications.

The experiments are conducted in some open-source simulators like Brian [39] and BindsNET [40], and we report the experiment results in terms of classification accuracy, learning efficiency, and robustness in the following sections. Moreover, in order to further exhibit the learning efficiency and robustness of our BioSNet, we conducted the same experiments on two previous unsupervised SNN algorithms in [16] and [15]. The related experiment results are denoted by Daniel2019 and D&C2015 respectively in the following part of this paper.

A. Classification Accuracy

We trained our network with only a single pass through the training data, meaning the networks are trained for 60,000 and 124,800 iterations respectively on MNIST and EMNIST training set. Then, we tested our networks on testing set of MNIST and EMNIST. The results are reported in TABLE III along with the setting of $(FilterN_1, FilterN_2, FilterN_3)$ and $n_{neurons}$, the total number of neurons in LC layers of all three channels. Note

that $(FilterN_1, FilterN_2, FilterN_3) = (3200, 800, 400)$ and $n_{neurons} = 10,000$ are the default setting of the following experiments in Section IV. Apparently, classification accuracy increases as the network size increases, which is compatible with the biological characteristics of the human brain.

The average test confusion matrix for our BioSNet with $n_{neurons} = 10,000$ is shown in Fig. 7. Every single classification result belongs to one of the tiles and its position is determined by the actual class and the predicted class. As is shown in Fig. 7(a), the most common confusion on MNIST is mistaking the digits ‘4’ and ‘7’ as ‘9’. Similarly, as can be seen in Fig. 7(b), the most common confusion on EMNIST are interchanging the letters ‘H’ and ‘K’ and interchanging the letters ‘F’ and ‘P’. The possible cause for that is their similarity. For example, when a neuron whose represented prototypical input is the digit ‘9’ receives an image of ‘4’, it’s highly possible to fire as well because of the similarity between ‘9’ and ‘4’.

For comparison, the testing results of some current unsupervised SNNs are shown in TABLE IV. Among all considered unsupervised SNNs, our BioSNet acquires the second-best testing results next only to [17] which incorporate the ‘forgetting’ of human brain into SNN to improve the classification accuracy. However, the method used in [17] also undermines the learning efficiency of SNN due to this ‘forgetting’. Unlike [17], the BioSNet performs superior learning efficiency in addition to favorable classification accuracy, which would be shown in detail in the Section IV-B. Concretely, our BioSNet is trained with only a single pass through the training data to achieve this classification accuracy, while some SNNs like [15][17][41] need to

TABLE III
TEST ACCURACY RESULTS FOR BIOSNET WITH VARYING SIZE

$(FilterN_1, FilterN_2, FilterN_3)$	n_{neuron}	MNIST	EMNIST
(800, 200, 100)	2,500	94.25%	73.93%
(1600, 400, 200)	5,000	95.16%	76.45%
(3200, 800, 400)	10,000	95.74%	77.91%

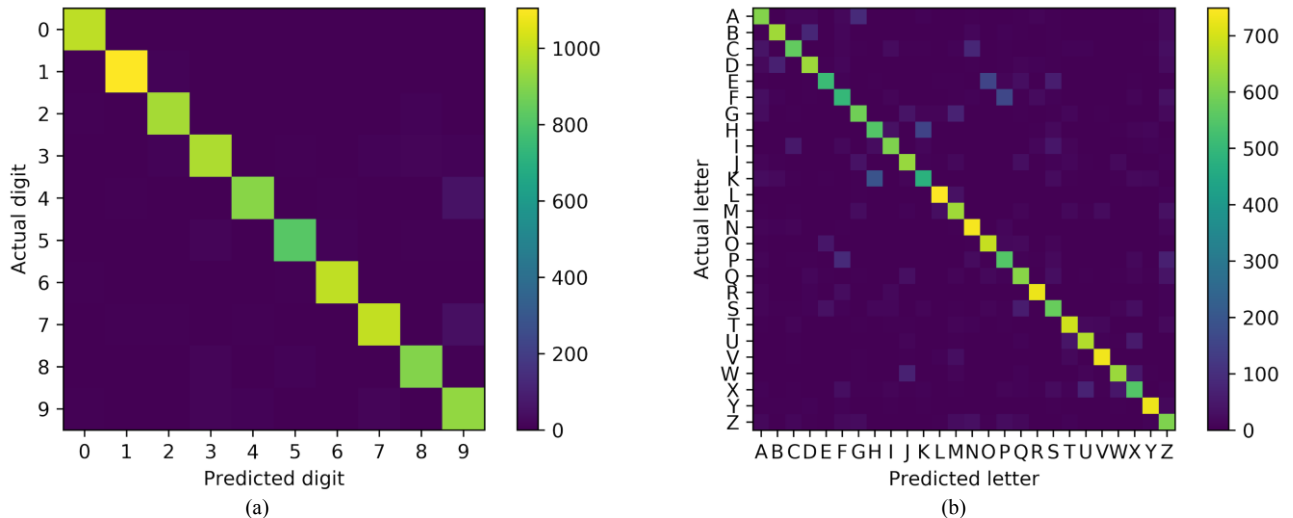


Fig. 7. Average confusion matrix of the testing results. (a) Confusion matrix over 10,000 handwritten digits in the MNIST testing set. (b) Confusion matrix over 20,800 handwritten letters in the EMNIST testing set.

TABLE IV
COMPARISON OF CURRENT UNSUPERVISED SNNs ON MNIST/EMNIST

Paper	Neuron Model	Network Architecture	Decoding Mechanism	MNIST	EMNIST
Ours	MRON model	Biomimetic SNN	VFA decoding layer	95.74%	77.91%
Daniel2019 [16]	Current-based LIF model	Locally-connected SNN	2-gram method	95.07%	69.73%
D&C2015 [15]	Conductance-based LIF model	Fully-connected SNN	Traditional voting mechanism	95.00%	47.41%
Querlioz et al. 2011 [41]	Current-based LIF model	Fully-connected SNN	Traditional voting mechanism	93.50%	/
Lammie et al. 2018 [43]	Izhikevich neuron model	Fully-connected SNN	Temporally decoding	94.00%	/
Allred et al. 2016 [43]	Conductance-based LIF model	Fully-connected SNN	Traditional voting mechanism	85.90%	/
Panda et al. 2018 [17]	Current-based LIF model	Fully-connected SNN	Traditional voting mechanism	96.80%	/

be trained with multiple passes through the training data to achieve their best performances. Besides, it's also worth noting that most of SNNs listed in TABLE IV utilize similar number of neurons in networks except for [42] that utilizes less neurons due to its temporal encoding/decoding scheme and [43] that requires obviously larger network models, but our BioSNet reaches state-of-the-art results of all considered unsupervised SNNs.

B. Learning Efficiency

The learning efficiency of the network is reflected on the classification performances with the limited training samples. A SNN with high learning efficiency can utilize very limited learning samples to quickly grasp the internal similarities and features, then performing a good classification accuracy. To evaluate the learning efficiency of BioSNet, in Fig. 8 we report the testing results of the networks trained with varying number of training samples on MNIST.

As can be seen in Fig. 8(a), we compare our BioSNet (with $n_{neurons} = 10,000$) with Daniel2019 and D&C2015. These three SNNs is similar in size (Concretely, 9,000 neurons are used in Daniel2019 and 12,800 neurons are used in D&C2015), but our BioSNet exhibits much more superior learning efficiency. The testing results of our BioSNet can achieve nearly 65%, 80%, and 90% accuracy after the training with only 100,

500, and 2500 samples, while Daniel 2019 just achieves nearly 10%, 30%, and 70% accuracy with 100, 500, and 2500 training samples, and worst of all, D&C2015 only reaches nearly 42% accuracy with even 10,000 training samples.

Besides, in Fig. 8(b) we also compare the learning efficiency of the BioSNet in different size. Surprisingly, the BioSNet in larger size performs better learning efficiency, which is contrary to our general idea that larger and more complicated networks tend to need more training samples to converge. However, this characteristic of BioSNet is corresponding to the human brain because more complicated brain system surely possesses higher-level learning capability to handle the task with less learning materials and time. The likely explanation is that because we fixed $Size_{ACL}$ to be reasonable value, the BioSNet in larger size actually consists of more areas of ACL, leading to its higher learning efficiency performance.

C. Robustness

In order to test the trained network's robustness against external interference and damage, we randomly deleted their STDP-modifiable synapses and neurons in LC layers respectively with probability ρ_{delete} . Here we report the testing results of the BioSNet, Daniel2019, and D&C2015 with varying ρ_{delete} of neuron/synapse deletion in Fig. 9. As can be seen in Fig. 9, the three SNNs without any neuron/synapse deletion

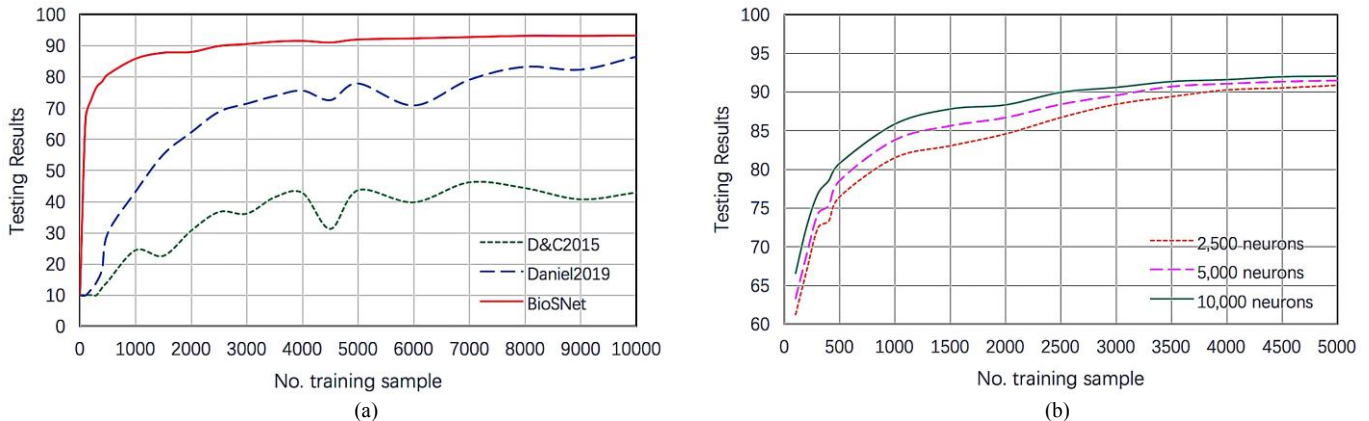


Fig. 8. The testing results of the networks trained with varying number of training samples on MNIST data set. (a) Comparison of learning efficiency among Daniel2019, D&C2015, and BioSNet. (b) Comparison of learning efficiency among three BioSNet models with different number of neurons in the LC layers.

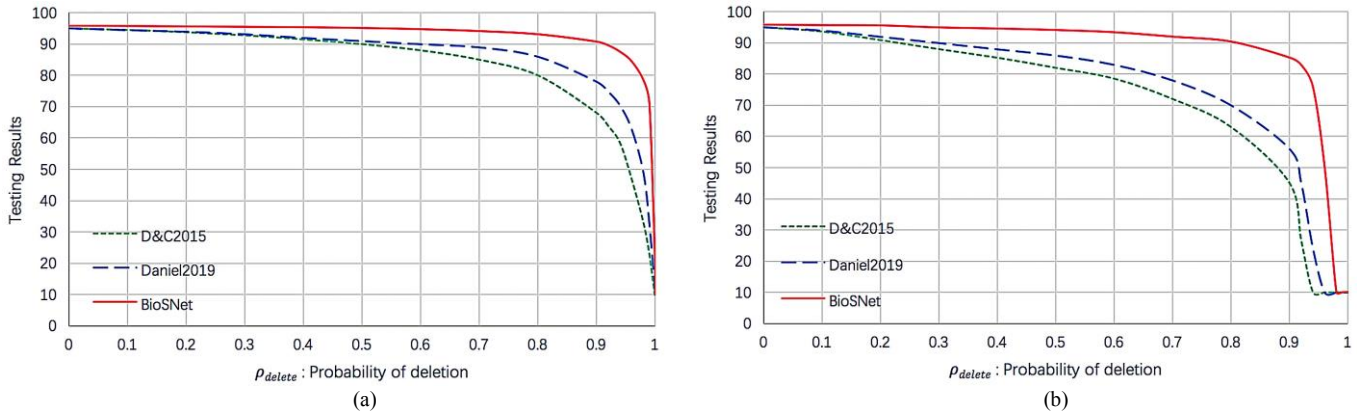


Fig. 9. Comparison of robustness among Daniel2019, D&C2015, and BioSNet. (a) The testing results with varying ρ_{delete} of neuron deletion on MNIST data set. (b) The testing results with varying ρ_{delete} of synapse deletion on MNIST data set.

maintain the accuracy of about 95% on MNIST, while increasing ρ_{delete} leads to a smooth degradation in testing result.

Fig. 9(a) shows the testing results after deleting neurons with probability ρ_{delete} and our BioSNet performs the best robustness. BioSNet maintains nearly 90% and 85% accuracy respectively with even 90% and 95% of neurons deleted, while Daniel2019 and D&C2015 maintain nearly 85% and 80% accuracy with only 80% of neurons deleted. Similarly, Fig. 9(b) shows the testing results after deleting synapses with probability ρ_{delete} and our BioSNet still performs the best robustness among them. BioSNet maintains nearly 85% and 75% accuracy respectively with even 90% and 95% of synapses deleted, while Daniel2019 and D&C2015 just maintain nearly 70% and 63% accuracy with only 80% of synapses deleted. These properties will make our network highly resilient to damage when implemented in hardware.

Apparently, compared with the deletion of neurons, the deletion of synapses has severer impact on the performance of the network, perhaps because randomly deleting synapses causes damage on all neurons and finally no neuron can work effectively. That can also explain why the testing results in Fig.9(b) decrease to 0 dramatically even without deleting all synapses.

V. DISCUSSION

Although the existing methods in MRON have enhanced the performance of our BioSNet significantly, there are still many development spaces in different aspects. For example, in the memory-reserved rules of the neurons, we could utilize the difference of transmitter $\delta_{i(t)}$ in the beginning and end of a certain period of time to determine the neuron's behavior. Through this method, we can obtain good results without much more computation required. Then, to pursue the further improvements of the network performance, we could change the operating conditions such as comparing the time integrals of membrane potential v_t to determine the time of operation, we could change the amount of PSP (postsynaptic potential) with memory effect to a continuous value, and we also could change the adjustment amount to a function of leakage current and membrane potential. Besides, we can further improve the performance of BioSNet by increasing the network size or adding extra layer to learn more abstract features. Note that it is necessary to balance the

increase in network computation and the benefits we get through above adjustments.

Admittedly, the learning of human brain is mysterious and profound. We cannot explain the process of learning and cognition in human brain very clearly, but our proposed BioSNet makes use of currently known theories of the human brain and integrates the advantages of modern machine learning algorithms and the biomimetic models based on neuroscience. Besides, some scholars recently argued that the innate architecture of the human brain could be more important for human's intelligence than the process of learning [44], which encourages us to research and find more biomimetic and effective network architecture. Moreover, in this paper, BioSNet achieved good performance with efficient neuron model and biomimetic network architecture while we use very basic STDP as the learning rule of the network. We encourage researchers to propose more advanced learning methods on our designed network and hope that more researchers will be able to notice the potential of it. Under the guidance of neuroscience, we are moving towards superior artificial intelligence.

VI. CONCLUSION

In this paper, BioSNet, an unsupervised biomimetic SNN with superior learning efficiency and high robustness, is proposed. The main distinctions of the BioSNet consists of three innovations: a flexible spiking neuron model named MRON inspired by 'recognition memory' of the human brain, an efficient and robust biomimetic network architecture combined with proposed ACL procedures, and an effective VFA decoding layer stemming from traditional voting mechanism. These innovations combined with the training strategies mentioned in Section III-E all contribute to the birth of BioSNet and make it perform state-of-the-art classification accuracy, superior learning efficiency, and high robustness. Specifically, we reached 95.74% and 77.91% classification accuracy respectively on MNIST and EMNIST data set, and the BioSNet that is trained with just 2500 training samples or suffers from random deletion of neuron/synapse with probability $\rho_{delete} \approx 0.9$ can still achieve the classification accuracy more than 90% on MNIST data set. Besides, all these proposed methods don't possess strict requirements for other integrates of SNN, which means that these

methods can contribute to improvement independently or concertedly and even can be potentially more powerful when combined with other SNN architectures.

With its high learning efficiency and robustness, the BioSNet can be applied to various applications limited by insufficient training samples or harsh working environment. Moreover, BioSNet, as a highly biomimetic SNN inspired by biological characteristics, has strong biological plausibility as well, meaning it could be a help to study the inner mystery of the human brain.

REFERENCES

- [1] Sendhoff, Bernhard, et al., eds. *Creating brain-like intelligence: from basic principles to complex intelligent systems*. Vol. 5436. Springer, 2009.
- [2] Vincent C. Müller. (2014) Risks of general artificial intelligence. *Journal of Experimental & Theoretical Artificial Intelligence* 26:3, pages 297-301.
- [3] Sporea, Ioana, and André Grüning. "Supervised learning in multilayer spiking neural networks." *Neural computation* 25.2 (2013): 473-509.
- [4] Roy, Subhrajit, and Arindam Basu. "An online unsupervised structural plasticity algorithm for spiking neural networks." *IEEE transactions on neural networks and learning systems* 28.4 (2016): 900-910.
- [5] Zhu, Xiaojin, and Andrew B. Goldberg. "Introduction to semi-supervised learning." *Synthesis lectures on artificial intelligence and machine learning* 3.1 (2009): 1-130.
- [6] Zhang, Wenrui, and Peng Li. "Information-theoretic intrinsic plasticity for online unsupervised learning in spiking neural networks." *Frontiers in neuroscience* 13 (2019).
- [7] Masquelier, Timothée, and Simon J. Thorpe. "Unsupervised learning of visual features through spike timing dependent plasticity." *PLoS computational biology* 3.2 (2007): e31.
- [8] Handrich, Sebastian, et al. *Combining Supervised, Unsupervised, and Reinforcement Learning in a Network of Spiking Neurons. Advances in Cognitive Neurodynamics (II)*. 2011:163-176
- [9] Rueckauer, Bodo, et al. "Conversion of continuous-valued deep networks to efficient event-driven networks for image classification." *Frontiers in neuroscience* 11 (2017): 682.
- [10] Rueckauer, Bodo, et al. "Theory and tools for the conversion of analog to spiking convolutional neural networks." *arXiv preprint arXiv:1612.04052* (2016).
- [11] Xie, Xiuwei, et al. "Efficient training of supervised spiking neural network via accurate synaptic-efficiency adjustment method." *IEEE transactions on neural networks and learning systems* 28.6 (2016): 1411-1424.
- [12] McKennoch, Sam, Dingding Liu, and Linda G. Bushnell. "Fast modifications of the spikeprop algorithm." *The 2006 IEEE International Joint Conference on Neural Network Proceedings*. IEEE, 2006.
- [13] Ponulak, Filip, and Andrzej Kasiński. "Supervised learning in spiking neural networks with ReSuMe: sequence learning, classification, and spike shifting." *Neural computation* 22.2 (2010): 467-510.
- [14] Wade, John J., et al. "SWAT: a spiking neural network training algorithm for classification problems." *IEEE Transactions on Neural Networks* 21.11 (2010): 1817-1830.
- [15] Diehl, Peter U., and Matthew Cook. "Unsupervised learning of digit recognition using spike-timing-dependent plasticity." *Frontiers in computational neuroscience* 9 (2015): 99.
- [16] Saunders, Daniel J., et al. "Locally Connected Spiking Neural Networks for Unsupervised Feature Learning." *arXiv preprint arXiv:1904.06269* (2019).
- [17] Panda, Priyadarshini, et al. "Asp: Learning to forget with adaptive synaptic plasticity in spiking neural networks." *IEEE Journal on Emerging and Selected Topics in Circuits and Systems* 8.1 (2017): 51-64.
- [18] Falez, Pierre, et al. "Multi-layered Spiking Neural Network with Target Timestamp Threshold Adaptation and STDP." *arXiv preprint arXiv:1904.01908* (2019).
- [19] Tavanaei, Amirhossein, and Anthony S. Maida. "Multi-layer unsupervised learning in a spiking convolutional neural network." *2017 International Joint Conference on Neural Networks (IJCNN)*. IEEE, 2017.
- [20] Kheradpisheh, Saeed Reza, et al. "STDP-based spiking deep convolutional neural networks for object recognition." *Neural Networks* 99 (2018): 56-67.
- [21] Hodgkin, Alan L., and Andrew F. Huxley. "A quantitative description of membrane current and its application to conduction and excitation in nerve." *The Journal of physiology* 117.4 (1952): 500-544.
- [22] Izhikevich, Eugene M. "Simple model of spiking neurons." *IEEE Transactions on neural networks* 14.6 (2003): 1569-1572.
- [23] Jeyasothy, Abeegithan, Suresh Sundaram, and Narasimhan Sundararajan. "Sefron: A new spiking neuron model with time-varying synaptic efficacy function for pattern classification." *IEEE transactions on neural networks and learning systems* 30.4 (2018): 1231-1240.
- [24] Nossenson, Nir, Ari Magal, and Hagit Messer. "Detection of stimuli from multi-neuron activity: Empirical study and theoretical implications." *Neurocomputing* 174 (2016): 822-837.
- [25] Fan, Deliang, et al. "Hierarchical temporal memory based on spin-neurons and resistive memory for energy-efficient brain-inspired computing." *IEEE transactions on neural networks and learning systems* 27.9 (2015): 1907-1919.
- [26] Squire, Larry R., John T. Wixted, and Robert E. Clark. "Recognition memory and the medial temporal lobe: a new perspective." *Nature Reviews Neuroscience* 8.11 (2007): 872.
- [27] Bear, Mark F., B. W. Connors, and M. A. Paradiso. *Neuroscience: Exploring the Brain*, 3rd Edition. *Neuroscience: exploring the brain*. Lippincott Williams & Wilkins, 2007:112-120
- [28] Hari, R. "Human Brain Function." *Trends in Cognitive Sciences* 2.2(1998):75-76.
- [29] Szegedy, Christian, et al. "Going deeper with convolutions." *Proceedings of the IEEE conference on computer vision and pattern recognition*. 2015.
- [30] Morrison, Abigail, Ad Aertsen, and Markus Diesmann. "Spike-timing-dependent plasticity in balanced random networks." *Neural computation* 19.6 (2007): 1437-1467.
- [31] Chen, Yu-hsin, et al. "Locally-connected and convolutional neural networks for small footprint speaker recognition." *Sixteenth Annual Conference of the International Speech Communication Association*. 2015.
- [32] McClelland, James L., David E. Rumelhart, and PDP Research Group. *Parallel distributed processing*. Vol. 2. Cambridge, MA: MIT press, 1987. *Explor. Microstruct. Cogn.* 2, 1–567.
- [33] Kohonen, Teuvo. "The self-organizing map." *Proceedings of the IEEE* 78.9 (1990): 1464-1480.
- [34] Fritzsche, Bernd. "A growing neural gas network learns topologies." *Advances in neural information processing systems*. 1995.
- [35] LeCun, Yann, Corinna Cortes, and C. J. Burges. "Mnist handwritten digit database. AT&T Labs." (2010).
- [36] Cohen, Gregory, et al. "EMNIST: an extension of MNIST to handwritten letters." *arXiv preprint arXiv:1702.05373* (2017).
- [37] Diehl, Peter U., et al. "Fast-classifying, high-accuracy spiking deep networks through weight and threshold balancing." *2015 International Joint Conference on Neural Networks (IJCNN)*. IEEE, 2015.
- [38] Neil, Daniel, Michael Pfeiffer, and Shih-Chii Liu. "Learning to be efficient: Algorithms for training low-latency, low-compute deep spiking neural networks." *Proceedings of the 31st annual ACM symposium on applied computing*. ACM, 2016.
- [39] Goodman, Dan FM, and Romain Brette. "The brain simulator." *Frontiers in neuroscience* 3 (2009): 26.
- [40] Hazan, Hananel, et al. "BindsNET: A machine learning-oriented spiking neural networks library in Python." *Frontiers in neuroinformatics* 12 (2018): 89.
- [41] Querlioz, Damien, Olivier Bichler, and Christian Gamrat. "Simulation of a memristor-based spiking neural network immune to device variations." *The 2011 International Joint Conference on Neural Networks*. IEEE, 2011.
- [42] Lammie, Corey, Tara Hamilton, and Mostafa Rahimi Azghadi. "Unsupervised character recognition with a simplified fpga neuromorphic system." *2018 IEEE International Symposium on Circuits and Systems (ISCAS)*. IEEE, 2018.
- [43] Allred, Jason M., and Kaushik Roy. "Unsupervised incremental stdp learning using forced firing of dormant or idle neurons." *2016 International Joint Conference on Neural Networks (IJCNN)*. IEEE, 2016.
- [44] Zador, Anthony M. "A critique of pure learning and what artificial neural networks can learn from animal brains." *Nature communications* 10.1 (2019): 1-7.



Mingyuan Meng received the B.E. degree in electronic information science and technology from Tsinghua University, Beijing, China, in 2018.

He is currently a hired researcher with the School of Electronics and Information Technology, Sun Yat-Sen University, Guangzhou, China. His current research interests include machine learning, neural networks, and pattern recognition.



Xingyu Yang is currently pursuing the graduate degree with the School of Electronic Information and Engineering, Sun Yat-Sen University of China, Guangzhou, China, in 2019.

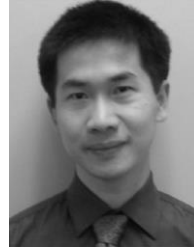
Her current research interests include spike neural networks, spike neuron models, and their hardware implementation.



Shanlin Xiao (M'19) received the B.S. degree in communications engineering and the M.S. degree in communications and information systems from the University of Electronic Science and Technology of China (UESTC), Chengdu, China, in 2009 and 2012, respectively. He received his Ph.D. degree in Communications and

Computer Engineering from the Tokyo Institute of Technology, Tokyo, Japan, in 2017.

He is currently an associate research professor at the School of Electronics and Information Technology in Sun Yat-Sen University, Guangzhou, China. His research interests include domain-specific architecture for artificial intelligence and neuromorphic computing.



Zhiyi Yu (SM'16) received the B.S. and M.S. degrees in EE from Fudan University, China, in 2000 and 2003, respectively, and the Ph.D. degree in ECE from the University of California at Davis, CA, USA, in 2007.

He was with IntellaSys Corporation, CA, USA, from 2007 to 2008. From 2009 to 2014, he was an associate professor in the Department of Microelectronics, Fudan University, China. Currently, he is a professor in the school of electronics and information technology, Sun Yat-sen University, China. His research interests include digital VLSI design and computer architecture.

Dr. Yu serves as TPC member on many conference committees, such as the ASSCC, VLSI-SOC, ISLPED, APSIPA, SASIM.